



HAL
open science

Electron magnetic reconnection without ion coupling in Earth's turbulent magnetosheath

T. D. Phan, Jonathan P. Eastwood, M. A. Shay, J. F. Drake, B. U. Ö.
Sonnerup, M. Fujimoto, P. A. Cassak, M. Oieroset, J. L. Burch, R. B.
Torbert, et al.

► **To cite this version:**

T. D. Phan, Jonathan P. Eastwood, M. A. Shay, J. F. Drake, B. U. Ö. Sonnerup, et al.. Electron magnetic reconnection without ion coupling in Earth's turbulent magnetosheath. *Nature*, 2018, 557, pp.202-206. 10.1038/s41586-018-0091-5 . hal-01895687

HAL Id: hal-01895687

<https://hal.science/hal-01895687v1>

Submitted on 1 Oct 2024

HAL is a multi-disciplinary open access archive for the deposit and dissemination of scientific research documents, whether they are published or not. The documents may come from teaching and research institutions in France or abroad, or from public or private research centers.

L'archive ouverte pluridisciplinaire **HAL**, est destinée au dépôt et à la diffusion de documents scientifiques de niveau recherche, publiés ou non, émanant des établissements d'enseignement et de recherche français ou étrangers, des laboratoires publics ou privés.

1 **Electron Magnetic Reconnection Without Ion Coupling in Earth's Turbulent**
2 **Magnetosheath**

3 T. D. Phan¹, J. P. Eastwood², M. A. Shay³, J. F. Drake⁴, B. U. Ö. Sonnerup⁵, M. Fujimoto⁶, P. A.
4 Cassak⁷, M. Øieroset¹, J. L. Burch⁸, R. B. Torbert⁹, A. C. Rager^{10,11}, J. C. Dorelli¹¹, D. J.
5 Gershman¹¹, C. Pollock¹², P. S. Pyakurel³, C. C. Haggerty³, Y. Khotyaintsev¹³, B. Lavraud¹⁴, Y.
6 Saito⁶, M. Oka¹, R. E. Ergun¹⁵, A. Retino¹⁶, O. Le Contel¹⁶, M. R. Argall⁹, B. L. Giles¹¹, T. E.
7 Moore¹¹, F. D. Wilder¹⁵, R. J. Strangeway¹⁷, C. T. Russell¹⁷, P. A. Lindqvist¹⁸, and W. Magnes¹⁹

8
9 ¹Space Sciences Laboratory, University of California, Berkeley, CA, USA

10 ²The Blackett Laboratory, Imperial College London, London, UK

11 ³University of Delaware, Newark, DE, USA

12 ⁴University of Maryland, College Park, MD, USA

13 ⁵Dartmouth College, Hanover, NH, USA

14 ⁶ISAS/JAXA, Japan

15 ⁷West Virginia University, Morgantown, WV, USA

16 ⁸Southwest Research Institute, San Antonio TX, USA

17 ⁹University of New Hampshire, Durham, NH, USA

18 ¹⁰Catholic University of America, Washington DC, USA

19 ¹¹NASA Goddard Space Flight Center, Greenbelt, MD, USA

20 ¹²Denali Scientific, Healy AK, USA

21 ¹³Swedish Institute of Space Physics, Uppsala, Sweden

22 ¹⁴Institut de Recherche en Astrophysique et Planétologie, Université de Toulouse, France

23 ¹⁵University of Colorado LASP, Boulder, Colorado, USA

24 ¹⁶CNRS/Ecole Polytechnique, Paris, France

25 ¹⁷University of California, Los Angeles, Los Angeles, CA, USA

26 ¹⁸Royal Institute of Technology, Stockholm, Sweden

27 ¹⁹Space Research Institute, Austrian Academy of Sciences, Graz, Austria

28

29

30

31

32 **Magnetic reconnection is a magnetic-to-particle energy conversion process fundamental to**
33 **many space and laboratory plasma systems. In the standard model of reconnection, this**
34 **process occurs in a minuscule electron-scale diffusion region around an X-line^{1,2}. On larger**
35 **scales, the ions couple to the newly-reconnected field lines and are ejected away from the X-**
36 **line in the form of bi-directional ion jets at the ion Alfvén speed³⁻⁵. Much of the energy**
37 **conversion occurs in spatially extended ion exhausts downstream of the diffusion region⁶.**
38 **In turbulent plasmas, which contain a large number of small-scale current sheets,**
39 **reconnection has long been suggested to play a major role in the dissipation of turbulent**
40 **energy at kinetic scales⁷⁻¹¹. However, experimental evidence for reconnection plasma jetting**
41 **in small-scale turbulent plasmas has so far been lacking. Here we report the discovery in**
42 **Earth's turbulent magnetosheath of an electron-scale current sheet where diverging bi-**
43 **directional super-ion-Alfvénic electron jets, parallel electric fields, and enhanced magnetic-**
44 **to-particle energy conversion were observed. Contrary to the standard reconnection**
45 **picture, the thin reconnecting current sheet was not embedded in a wider ion-scale current**
46 **layer and no ion jets were detected. Observations of this and other similar, but**
47 **unidirectional, electron jet events without ion reconnection signatures reveal a new form of**
48 **reconnection that can drive turbulent energy transfer and dissipation in electron-scale**
49 **current sheets without ion coupling.**

50

51

52 Turbulent magnetosheath regions downstream of Earth's quasi-parallel bow shock often contain
53 hundreds of small-scale current sheets in which reconnection could potentially occur^{9,10,12}
54 (Figure 1c). Many are thin (ion inertial length scales or smaller), typically convecting past an
55 observing spacecraft in a few seconds or less. If standard reconnection (Figure 1a) were to
56 operate in turbulent current sheets, the ion jets in the extended exhausts should be the easiest
57 reconnection signature to detect. Although electric field and magnetic field structures consistent
58 with standard reconnection have been reported^{9,10}, in situ plasma measurements of the jets were
59 not obtained for these thin current sheets because the data resolution using previous instruments
60 (typically a few seconds per velocity measurement) was not sufficient to determine their
61 presence or absence.

62 The four-spacecraft MMS mission, launched in 2015 and designed to reveal the kinetic physics
63 of reconnection in near-Earth space, is flying in an electron-scale (~ 7 -10 km) tetrahedral
64 formation. It measures 3-D electron and ion distributions at up to 7.5 ms and 37.5 ms
65 resolution¹³, respectively, which are 400 times and 80 times better resolved than previously
66 available data. MMS observations of turbulent magnetosheath current sheets have revealed thin
67 current sheets¹⁴, fast electron flows^{15,16}, and electron heating^{12,16}. These characteristics are
68 somewhat similar to those observed in the standard reconnection electron diffusion region in
69 large-scale current sheets at the magnetopause^{2,17} and in the laminar magnetosheath (that
70 originate in the solar wind)^{18,19}. However, ion jets, which should occur over a larger scale and
71 therefore be more easily observed if standard reconnection is present in turbulent magnetosheath
72 current sheets, remain elusive. This raises the question of whether fast electron flows in thin
73 turbulent magnetosheath current sheets are produced by some process(es) besides reconnection.

74 Here we report the serendipitous simultaneous multi-spacecraft detection of oppositely directed
75 super-ion-Alfvénic electron jets, parallel electric fields, and magnetic-to-particle energy
76 conversion in an electron-scale current sheet in the magnetosheath, providing direct evidence for
77 reconnection without ion-scale coupling in turbulence.

78 Figure 2a-c shows the large-scale context of the MMS observations in the subsolar
79 magnetosheath region on December 9, 2016, 8:58-9:43 UT, with large fluctuations in both the
80 magnetic field magnitude (Panel a) and its components (Panel b). Figures 2d-2g reveal these
81 fluctuations to be sharp changes in the magnetic field associated with large current density
82 spikes, many with $|\mathbf{j}| > 2 \mu\text{A}/\text{m}^2$ and comparable to peak current densities observed in the
83 electron diffusion region at Earth's magnetopause^{2,17,20}. Such large current densities across
84 magnetic field variations of a few tens of nT imply current sheet widths of a few tens of
85 kilometers or less, i.e., below the ion inertial length (and ion gyroradius) of ~ 50 km in this
86 interval. Closer inspection of the current density and magnetic field variations throughout the
87 interval in Figures 2 reveals a range of current sheet thicknesses, i.e., many but not all are of sub-
88 ion scales.

89 In order to distinguish the regular fast electron flows associated with any thin current sheet from
90 electron jets due to reconnection, data should be examined in a current sheet (LMN) coordinate
91 system. The current sheet normal points along \mathbf{N} , \mathbf{L} is along the anti-parallel magnetic field
92 direction, and $\mathbf{M} = \mathbf{N} \times \mathbf{L}$ is in the out-of-plane (X-line) direction (Figure 1a). In such a frame, the
93 main current is in the M direction, while the bi-directional reconnection outflows are in the $\pm L$
94 directions (Figure 1b). “Smoking gun” evidence for reconnection would be the simultaneous
95 detection of oppositely directed plasma outflow jets by two spacecraft located on opposite sides
96 of the X-line⁴.

97 Such an event was captured at $\sim 09:03:54$ UT, when $|\mathbf{j}|$ reached $\sim 3\mu\text{A}/\text{m}^2$ (red arrow in Fig. 2g).
98 Figure 3 shows in detail this current sheet, which had a magnetic shear of 14° (the guide field B_M
99 ~ 40 nT, compared to anti-parallel field $|B_L| \sim 5$ nT). Four spacecraft timing analysis finds the
100 current sheet thickness to be only 4 km (or 4 electron skin depths, d_e), determined from the 45
101 ms crossing duration (between the vertical dashed lines in Figure 3) and the 95 km/s convection
102 speed (V_N) of the current sheet.

103

104 Inside this electron-scale current sheet, both MMS 3 (left) and MMS 1 (right) observed fast out-
105 of-plane electron flows $V_{eM} \sim 900$ km/s (Fig. 3c and 3m) that produced the main current j_M (Fig.
106 3d and 3n) and the associated B_L reversal (Fig. 3a and 3k). The V_{eM} speed is comparable to the
107 inflow electron Alfvén speed, V_{AeL} , of 1000 km/s based on $B_L \sim 5$ nT and plasma density of 20
108 particles/cm³.

109

110 Coincident with the intense current layers, MMS 3 and MMS 1 simultaneously observed
111 oppositely directed electron jets in the outflow (L) direction, with $\Delta V_{eL} \sim +250$ km/s at MMS 3
112 (Fig. 3c) and ~ -450 km/s at MMS 1 (Fig. 3m), relative to an external V_{eL} flow of $\sim +150$ km/s.
113 These electron outflow jets were ~ 10 - 18 times the asymptotic ion Alfvén speed (based on B_L),
114 V_{AiL} , of ~ 25 km/s. As expected for a reconnection geometry with inflow from both sides, the
115 changes in B_L for MMS 1 are correlated with those in V_{eL} in the first part of the field change and
116 anti-correlated in the second half, while for MMS 3 the reverse holds. An exception to this
117 behavior is that MMS 3, but not MMS 1, observed a ΔV_{eL} (~ -300 km/s) flow at the right-hand
118 edge that is opposite to the main ΔV_{eL} flow (Fig. 3c). Simulations of standard reconnection with a

119 strong guide field have shown such ΔV_{eL} edge flow²¹. The lack of an edge flow at MMS 1 is
120 currently not understood.

121

122 The measurements of oppositely directed electron outflows at MMS 1 and MMS 3 are further
123 supported by the higher resolution (0.125 ms) measurements of the L component of the field line
124 velocity $\mathbf{E} \times \mathbf{B} / B^2$, which was negative at MMS 1 and positive at MMS 3 (except for a negative
125 dip at the right edge, similar to V_{eL}) (Fig. 3q and 3g). The $(\mathbf{E} \times \mathbf{B} / B^2)_L$ outflows were
126 predominantly perpendicular to the magnetic field due to the large B_M (Fig 3a and 3k); E_N (Fig.
127 3e and 3o), which is opposite at the 2 spacecraft, together with the dominant B_M , drives the
128 outflows. Crucially, MMS 3 was located 7.1 km in the +L direction relative to MMS 1 so that the
129 observations are consistent with diverging jets from a reconnection X-line located between the
130 two spacecraft as they pass through the reconnecting current sheet. There was no evidence for
131 ion jets (ΔV_{iL}) at the ion Alfvén speed (Fig. 3b,l) within the thin current sheet. That ion jets are
132 absent is not surprising, because the current sheet thickness was only 0.09 d_i (or 0.09 ion
133 gyroradii), and because the observations were made within 7 d_e of the X-line.

134

135 What is surprising, however, is that the electron-scale reconnecting current sheet was not
136 embedded inside a much larger ion-scale current sheet as would be expected (and observed) in
137 standard reconnection^{1,18-20,22} (Fig. 1a). The absence of an outer ion-scale current sheet can be
138 seen in Figures 3a and 3k (see also Extended Data Figure 1) which show B_L reaching its
139 asymptotic values immediately outside the thin current sheet.

140

141 Both spacecraft detected well-defined parallel electric fields (Fig. 3f and 3p), implying that the
 142 electron frozen-in condition $\mathbf{E}' = \mathbf{E} + \mathbf{V}_e \times \mathbf{B} = 0$ was violated. Furthermore, $\mathbf{j} \cdot \mathbf{E}'$ was positive (Fig.
 143 3j and 3t) and dominated by $j_{\parallel} E_{\parallel}$, indicating non-ideal magnetic-to-particle energy conversion²³
 144 characteristic of the electron diffusion region. However, unlike standard reconnection where
 145 most of the magnetic energy is converted into ion jetting and heating, here, half of the (6 eV)
 146 available magnetic energy per particle in the inflow regions, $m_e V_{AeL}^2$, goes into kinetic energy
 147 associated with ΔV_{eM} and ΔV_{eL} , flowing at 90% and 45% of the electron Alfvén speed V_{AeL} ,
 148 respectively. The remaining half (3 eV), if converted entirely into electron heating, would lead to
 149 a (3 eV) $(\gamma-1)/\gamma \approx 1$ eV electron temperature increase in the reconnecting current sheet²⁴, where γ
 150 = 5/3 is the ratio of specific heats. Such a small temperature increase would be not be discernable
 151 in the data (Fig. 3i and 3s).

152

153 Within the 21-minute burst data intervals shown in Figure 2a there were 34 other isolated current
 154 sheets with $|\mathbf{j}| > 2 \mu\text{A}/\text{m}^2$ which implies sub-ion-scale current sheet widths. Surprisingly, the
 155 majority of these current sheets had low magnetic shears (i.e., strong guide fields): 23 of the 34
 156 events had magnetic shear $< 45^\circ$. All 34 showed fast out-of-plane electron velocity V_{eM}
 157 consistent with the large current density j_M , but only 16 displayed clear super-ion-Alfvénic V_{eL}
 158 jets that could be related to reconnection. In each of these cases, all four spacecraft detected V_{eL}
 159 pointing in the same direction and were therefore embedded in the same jet. The scarcity of
 160 unambiguous reconnection events with divergent jets and the X-line located between the
 161 spacecraft is likely due to the small (~ 7 km or $7 d_e$) spacecraft separations.

162

163 We have found no evidence for reconnection ion jetting associated with any of the electron
164 outflow jet events, or in any other (including ion-scale thick) current sheets in the 21-minute
165 interval (see examples in Extended Data Figure 2). This finding is in stark contrast to standard
166 models of reconnection where the ion exhaust jets should be easier to detect than the electron
167 diffusion region because they extend large distances from the X-line.

168

169 The absence of ion reconnection signatures suggests that, in these turbulent magnetosheath
170 plasmas, there is insufficient space and/or time for the ions to couple to the magnetic structures.
171 This could occur not only because the current sheet widths are of electron scales, but also if the
172 overall dimensions of the current sheets are limited because ion coupling requires some
173 minimum lengths along the exhaust²⁵ (L) and X-line²⁶ (M) directions. A hybrid simulation study
174 of resistive reconnection with no guide field²⁵ suggests that ions become decoupled when the
175 length of the current sheet (in the L direction, e.g., Fig. 1c) falls below $\sim 10 d_i$. If such an
176 electron-ion decoupling scale also exists in strong guide field collisionless reconnection, though
177 potentially at a smaller scale than $10 d_i$, it could account for our observed lack of ion coupling in
178 magnetosheath reconnection, where the coherence scales of magnetic structures have been
179 reported²⁷ to be of the order of d_i .

180

181 The experimental discovery of electron-only reconnection reveals that reconnection operates
182 differently in current sheets with small overall dimensions. Our finding supports the long-held
183 idea that reconnection plays a role in dissipating energy associated with plasma turbulence in
184 space and astrophysical systems, although the scale for dissipation by reconnection would be at
185 the electron scale instead of the ion scale. In order to quantitatively assess the importance of

186 reconnection in dissipating turbulence energy in small systems, the basic properties of electron-
187 only reconnection (e.g., the rate, duration, and onset conditions of reconnection) will need to be
188 investigated both theoretically and observationally. They could differ significantly from our
189 knowledge based on the standard reconnection paradigm.

190
191
192

References

- 193 1. Vasyliunas, V. M. Theoretical models of magnetic merging, *Rev. Geophys*, **13**, 1, 303-
194 336, 1975.
- 195 2. Burch, J. L. *et al.* Electron-Scale Measurements of Magnetic Reconnection in Space,
196 *Science*, **352**, 1189-1199 (2016).
- 197 3. Paschmann, G. *et al.* Plasma acceleration at the earth's magnetopause: Evidence for
198 reconnection, *Nature* **282**, 243-246 (1979).
- 199 4. Phan, T. D. *et al.* Extended magnetic reconnection at the Earth's magnetopause from
200 detection of bi-directional jets, *Nature*, **404**, 848-850 (2000).
- 201 5. Gosling, J. T. *et al.* Direct evidence for magnetic reconnection in the solar wind near
202 1AU, *J. Geophys. Res.*, **100**, A1 (2005).
- 203 6. Petschek, H. E., Magnetic field annihilation, in *AAS-NASA Symposium on the Physics of*
204 *Solar Flares*, NASA Spec. Publ. SP-50, 425 (1964).
- 205 7. Matthaeus, W. H. and Lamkin, S. L. Turbulent magnetic reconnection, *Phys. Fluids*, **29**,
206 2513 (1986).
- 207 8. Servidio, S. *et al.* Magnetic reconnection in two-dimensional magnetohydrodynamic
208 turbulence. *Phys. Rev. Letters*, **102** (2009).
- 209 9. Retinò, A. *et al.* *In situ* evidence of magnetic reconnection in turbulent plasma, *Nature*
210 *Physics* **3**, 235 – 238 (2007).
- 211 10. Sundqvist, D. *et al.* Dissipation in Turbulent Plasma due to Reconnection in Thin Current
212 Sheets, *Phys. Rev. Lett.* **99**, (2007).
- 213 11. Haggerty, C. C. *et al.* Exploring the statistics of magnetic reconnection X-points in
214 kinetic particle-in-cell turbulence, *Physics of Plasmas*, **24**, 102308 (2017).
- 215 12. Chasapis, A. *et al.* Electron Heating at Kinetic Scales in Magnetosheath Turbulence,
216 *Astro. Phys. J.*, **836**, 2, 247-255 (2017).
- 217 13. Rager, A. C. *et al.* Electron crescent distributions as a manifestation of diamagnetic drift
218 in an electron scale current sheet: Magnetospheric Multiscale observations using new 7.5
219 ms Fast Plasma Investigation moments, *Geophys. Res. Lett.*, doi:
220 10.1002/2017GL076260 (2018).
- 221 14. Eriksson, E. *et al.* Strong current sheet at a magnetosheath jet: Kinetic structure and
222 electron acceleration, *J. Geophys. Res.*, **121**, 10, 9608-9618 (2016).
- 223 15. Yordanova, E. *et al.* Electron scale structures and magnetic reconnection signatures in the
224 turbulent magnetosheath, *Geophys. Res. Lett.*, **43**, 5969–5978 (2016).

- 225 16. Vörös, Z. *et al.* MMS observations of magnetic reconnection in the turbulent
226 magnetosheath, *J. Geophys. Res.*, in press, (2017).
- 227 17. Chen, L. J. *et al.* Electron energization and mixing observed by MMS in the vicinity of an
228 electron diffusion region during magnetopause reconnection, *Geophys. Res. Lett.*, **43**, 12,
229 6036-6043 (2016).
- 230 18. Phan, T. D. *et al.* Evidence for an elongated (> 60 ion skin depths) electron diffusion
231 region during fast magnetic reconnection, *Phys. Rev. Lett.*, **99**, 25 (2007).
- 232 19. Wilder, F. D. *et al.* Multipoint measurements of the electron jet of symmetric magnetic
233 reconnection with a moderate guide field, *Phys. Res. Lett.*, **118** (2017)
- 234 20. Burch, J. L. and Phan, T. D. Magnetic reconnection at the dayside magnetopause:
235 Advances with MMS, *Geophys. Res. Lett.*, **43**, 16, 8327-8338 (2016).
- 236 21. Pritchett, P. L. Geospace Environment Modeling magnetic reconnection challenge:
237 Simulations with a full particle electromagnetic code, *J. Geophys. Res.*, **106**, 3783-3798
238 (2001).
- 239 22. Shay, M. A. *et al.* Structure of the dissipation region during collisionless magnetic
240 reconnection, *J. Geophys. Res.*, **103**, A5, 9165-9176 (1998).
- 241 23. Zenitani, S. *et al.* New Measure of the Dissipation Region in Collisionless Magnetic
242 Reconnection, *Phys. Rev. Lett.* **106**, issue 19 (2011).
- 243 24. Shay, M. A. *et al.* Electron heating during magnetic reconnection: A simulation scaling
244 study, *Phys. Plasmas*, **21**, 122902:1-11 (2014).
- 245 25. Mandt, M. E. *et al.* Transition to whistler mediated magnetic reconnection, *Geophys. Res.*
246 *Lett.*, **21**, 1, 73-76 (1994).
- 247 26. Meyer, J. C. Structure of the diffusion region in three dimensional
248 magnetic reconnection, PhD thesis, University of Delaware (2015).
- 249 27. He, J. S. *et al.* Two-dimensional correlation functions for density and magnetic field
250 fluctuations in magnetosheath turbulence measured by the Cluster spacecraft, *J. Geophys.*
251 *Res.*, **116**, A6, CiteID A06207 (2011).
- 252 28. Torbert, R. B. *et al.* The FIELDS Instrument Suite on MMS: Scientific Objectives,
253 Measurements, and Data Products, *Space Sci. Rev.*, (2014).
- 254 29. Gosling, J. T. and Phan T. D. Magnetic reconnection in the solar wind at current sheets
255 associated with extremely small field shear angles, *Astrophys. J. L.*, **763** (2013).
- 256 30. Sonnerup, B. U. Ö., Cahill Jr., L. J. Magnetopause structure and attitude from Explorer
257 12 observations, *J. Geophys. Res.*, **96**, 72, 171 (1967).

258

259 **Acknowledgments.** We are grateful for the dedicated efforts of the MMS team. This work was
260 supported by NASA Contract No. NNG04EB99C at SwRI, which funded work at most of the co-
261 author institutions in the United States. The work at U.C. Berkeley was supported by NASA
262 grant NNX08AO83G. UK involvement at Imperial College was supported by STFC (UK) grant
263 ST/N000692/1. The French involvement (SCM instruments) on MMS is supported by CNES,
264 CNRS-INSIS and CNRS-INSU.

265 **Author Contributions** T. D. P. carried out the data analysis, interpretation, and manuscript
266 preparation. J.P.E, M.A.S, J.F.D, B.U.Ö.S., M.F., P.A.C., M.Ø., P.S.P., C.H., M.O, and A.R.
267 contributed to the data interpretation and manuscript preparation. J. L. B led the successful
268 design and operation of the MMS mission and contributed to the interpretation of the data.
269 A.C.R., J.C.D., D.J.G., C. P., B.L, B.L.G, T.E.M, and Y.S. contributed to the development,
270 operation, and interpretation of data from the Fast Plasma Instruments. R.B.T., R.E.E., Y.K.,
271 M.R.A., F.D.W. and P.A.L. contributed to the development, operation, and interpretation of data
272 from the electric field experiments. O.L.C. contributed to the development and operation of the
273 search-coil magnetometers. C.T.R., R.J.S, and W.M. contributed to the development and
274 operation of the fluxgate magnetometers.

275 **Author Information.** Reprints and permissions information is available at
276 www.nature.com/reprints. The authors declare no competing financial interests. Correspondence
277 and requests for materials should be addressed to T.D.P (phan@ssl.berkeley.edu).

278 **Data availability.** The entire MMS data set is publicly available on-line at
279 <https://lasp.colorado.edu/mms/sdc/public/>.

Main Figure Legends

280
281
282
283
284
285
286
287
288
289
290
291
292
293
294
295
296
297
298
299
300
301
302

Figure 1. Schematics contrasting (a) standard magnetic reconnection in large-scale current sheets and (b, c) electron-only reconnection in small-scale turbulence. The reconnection configurations in panels (a) and (b) are displayed in the current sheet (LMN) coordinate system. (a) In standard reconnection, the magnetic topology changes in the small electron diffusion region (EDR) around the X-line, but most of the magnetic-to-particle energy conversion happens in the extended exhausts, with bidirectional ion jetting and heating. The EDR width (along **N**) is of the order of an electron skin depth (d_e), while its length along $\pm L$ could be up to a fraction of an ion inertial length $d_i = 43 d_e$. The EDR is embedded in an ion diffusion region (IDR), while the magnetohydrodynamic-scale reconnection exhaust can extend thousands of d_i (along **L**) away from the X-line⁵. (b) Schematics of reconnection in an electron-scale current sheet involving only electrons, with no ion coupling. The entire current sheet is essentially the electron diffusion region having a single (electron) scale with embedded bi-directional super-ion-Alfvénic jets. Overlaid are MMS 1 and 3 trajectories through the current sheet relative to the X-line deduced based on the electron jet directions observed on 2016-12-09 at ~09:03:54 UT (and shown in Figure 3). MMS 1 and 3 were on opposite sides of the X-line detecting bi-directional electron jets. The slanted spacecraft trajectories take into account the likely motion (in the spacecraft frame) of the X-line due to the presence of an external electron flow along $+L$ of ~ 150 km/s. (c) Schematic showing the formation of multiple small (d_i)-scale magnetic structures and thin (d_e -scale) current sheets at their interfaces in turbulent plasmas, informed by turbulence simulations^{8,12}.

Figure 2. Overview of MMS 1 observations of turbulent current sheets in Earth’s subsolar magnetosheath region downstream of a quasi-parallel shock, showing the presence of large current density spikes ($>2 \mu\text{A}/\text{m}^2$) implying sub-ion-scale current sheets. The data is displayed in the geocentric solar ecliptic (GSE) coordinates. (a, b) The magnetic field magnitude and components. (c) The ion energy-time spectrogram of differential energy flux ($\text{eV s}^{-1} \text{cm}^{-2} \text{ster}^{-1} \text{eV}^{-1}$). (d-g) Zoomed-in (4-minute) interval showing the magnetic field, ion velocity, electron velocity, and current density computed from plasma measurements $\mathbf{j} = eN_e(\mathbf{V}_i - \mathbf{V}_e)$. Throughout the interval in panels a-c, the angle between the interplanetary magnetic field and X_{GSE} was less than 30° and the subsolar bow shock was quasi-parallel. The current density spike

312 at ~09:03:54 UT (indicated by the red arrow in panel g) is the bi-directional electron jet event to
313 be shown in detail in Figure 3. Red horizontal bars in panel a denote burst data intervals totaling
314 21 minutes selected by the MMS scientist-on-duty because they contained a large number of
315 high amplitude magnetic field fluctuations (with $\Delta\mathbf{B}/B \sim 0.5$) suggestive of current sheets that
316 could be prone to reconnection.

317

318 **Figure 3. MMS 1 and 3 simultaneous detections of oppositely directed super-ion-Alfvénic**
319 **electron jets, parallel electric fields, and enhanced magnetic-to-electron energy conversion**
320 **in an electron-scale current sheet.** The data for both spacecraft are shown in a common current
321 sheet (LMN) coordinate system determined for the MMS 3 crossing of the current sheet at
322 09:03:54.270 – 09:03:54.365 UT, with $\mathbf{L} = (-0.091, 0.87, 0.49)_{\text{GSE}}$, $\mathbf{M} = (-0.25, -0.49, 0.83)_{\text{GSE}}$,
323 and $\mathbf{N} = (0.96, -0.05, 0.27)_{\text{GSE}}$. (a,k) Magnetic field at 8196 samples/s (from merged fluxgate and
324 search-coil magnetometer measurements²⁸), with B_M shifted by -30 nT. (b,c and l,m) Ion and
325 electron velocity. The 7.5 ms electron and 37.5 ms ion data products were generated by
326 separating the individual energy sweeps used to form the nominal burst-mode distribution
327 functions. These data maintain sufficient angular coverage to recover accurate plasma moments
328 at 4 times the nominal temporal resolution¹³. (d,n) Current density from plasma measurements.
329 (e,o) Electric field²⁸ in the spacecraft frame at 8196 samples/s. (f,p) Electric field component
330 parallel to the magnetic field. (g,q) $\mathbf{E} \times \mathbf{B} / B^2$ velocity. (h) Electron density. (i) Electron
331 temperature. (j,t) $\mathbf{j} \cdot (\mathbf{E} + \mathbf{V}_e \times \mathbf{B})$. The LMN coordinate system was determined using a hybrid
332 minimum variance method which often works best in low magnetic shear current sheets²⁹. The
333 current sheet normal direction, \mathbf{N} , was determined from $\mathbf{B}_1 \times \mathbf{B}_2 / |\mathbf{B}_1 \times \mathbf{B}_2|$, where \mathbf{B}_1 and \mathbf{B}_2 are
334 the fields at the two edges of the current sheet. $\mathbf{M} = \mathbf{L}' \times \mathbf{N}$, where \mathbf{L}' is the maximum variance
335 direction from the minimum variance of the magnetic field³⁰. $\mathbf{L} = \mathbf{N} \times \mathbf{M}$. MMS 3 was located at
336 $L = +7.1$ km, $M = +3.3$ km, and $N = +1.6$ km relative to MMS1. Data from all 4 spacecraft are
337 shown in Extended Data Figure 3.

338

339

340

Extended Data Figure Legends

341
342
343
344
345
346
347
348
349
350
351
352
353
354
355
356
357
358
359
360
361
362
363
364
365
366
367
368
369
370
371

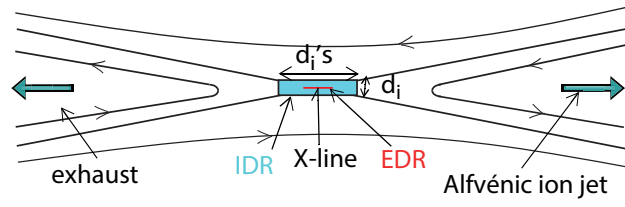
Extended Data Figure 1. Large-scale context of the thin current sheet shown in Figure 3, illustrating the fact that the electron-scale current sheet was a stand-alone current sheet not embedded inside an ion-scale current sheet. Data is shown in LMN coordinates determined for the thin current sheet and used in Figure 3. (a) Magnetic field. (b) Ion velocity. (c) Electron velocity. (d) $\mathbf{j} \cdot (\mathbf{E} + \mathbf{V}_e \times \mathbf{B})$. The thin reconnecting current sheet stands out in this interval, with nothing else approaching its current density or its value of $\mathbf{j} \cdot (\mathbf{E} + \mathbf{V}_e \times \mathbf{B})$. The absence of an ion-scale current sheet enveloping the electron-scale current sheet is indicated by the fact that $|B_L|$ reaches essentially its asymptotic values immediately outside the thin current sheet.

Extended Data Figure 2. Absence of reconnection ion jetting. The data is in GSE coordinates. (a) Magnetic field. (b) Ion velocity. (c) Y component of the ion velocity, V_{iy} , and Alfvén velocity, V_{Ay} . (d) Z component of the ion velocity, V_{iz} , and Alfvén velocity, V_{Az} . \mathbf{V}_A is relative to the reference velocity, density, and magnetic field values at the left edge of the data interval: $\mathbf{V}_A = \mathbf{B}_{\text{ref}}(1 - \alpha_{\text{ref}})^{1/2} (\mu_0 \rho_{\text{ref}})^{-1/2} - \mathbf{B}(1 - \alpha)^{1/2} (\mu_0 \rho)^{-1/2}$, where $\alpha = (\rho_{\parallel} / \rho_{\perp}) \mu_0 / B^2$ is the pressure anisotropy factor and ρ is the plasma mass density³. The expected speeds of the ion reconnection jets embedded inside many of the large magnetic shear current sheets are in the range of 100-200 km/s, based on B_L variations of the order of 20-40 nT (panel a). If present, such jets are readily recognized by back-to-back opposite correlations between ion velocity and magnetic field variation at the two edges of the current sheet as indications of pairs of rotational discontinuities emanating from the X-line⁵. These signatures are not seen here. What one finds instead in the data is either no correlation between components of \mathbf{V}_i and \mathbf{B} , or single correlation (or anti-correlation), indicative of Alfvénic structures¹⁶ rather than reconnection jetting.

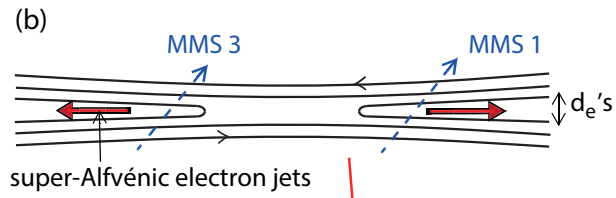
Extended Data Figure 3. Four-spacecraft observations of the reconnecting current sheet shown in Figure 3. A common current sheet LMN coordinate system (same as in Figure 3) was used for consistency, and supported by the fact that the LMN coordinates at individual spacecraft differ from each other by less than 4°. (a,b) L and M components of the magnetic field, (c,d) L and M components of the electron velocity. (e) M component of the current density. (f) L

372 component of the $\mathbf{E} \times \mathbf{B} / B^2$ velocity, (g) N component of the electric field. (h) electric field
 373 component parallel to the magnetic field, (i) $\mathbf{j} \cdot (\mathbf{E} + \mathbf{V}_e \times \mathbf{B})$, and (j) spacecraft locations relative to
 374 MMS 1, in km ($\sim d_e$). The B_L profiles (panel a) show that MMS 1 and 3 crossed the current sheet
 375 at essentially the same time, preceded by MMS 4 and followed by MMS 2. The fact that MMS 4
 376 exited the current sheet before MMS 2 entered it places an upper limit on the current sheet
 377 thickness, which is the 4.5 km separation distance between the 2 spacecraft along \mathbf{N} (panel f).
 378 This is consistent with the 4 km current sheet width determined from the motion and crossing
 379 duration of the current sheet. Inside the current sheet, MMS 4 detected a positive $(\mathbf{E} \times \mathbf{B} / B^2)_L$
 380 (except at the right edge) similar to MMS 3, whereas MMS 2 detected a negative $(\mathbf{E} \times \mathbf{B} / B^2)_L$
 381 similar to MMS 1. This indicates that there was a pair of spacecraft on each side of the X-line.
 382 All 4 spacecraft detected a predominantly negative E_{\parallel} . The parameter $\mathbf{j} \cdot (\mathbf{E} + \mathbf{V}_e \times \mathbf{B})$ was
 383 consistently positive at all 4 spacecraft throughout the current sheet, with the amplitude being
 384 lowest at MMS 2. MMS 2 also detected the largest guide field (B_M) compression, fastest ΔV_{eL}
 385 and $(\mathbf{E} \times \mathbf{B} / B^2)_L$ flows, slowest ΔV_{eM} and weakest E_{\parallel} , which together may suggest that MMS 2
 386 was furthest away from the X-line.

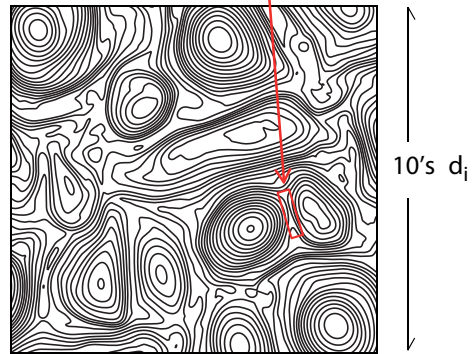
(a) Standard Magnetic Reconnection

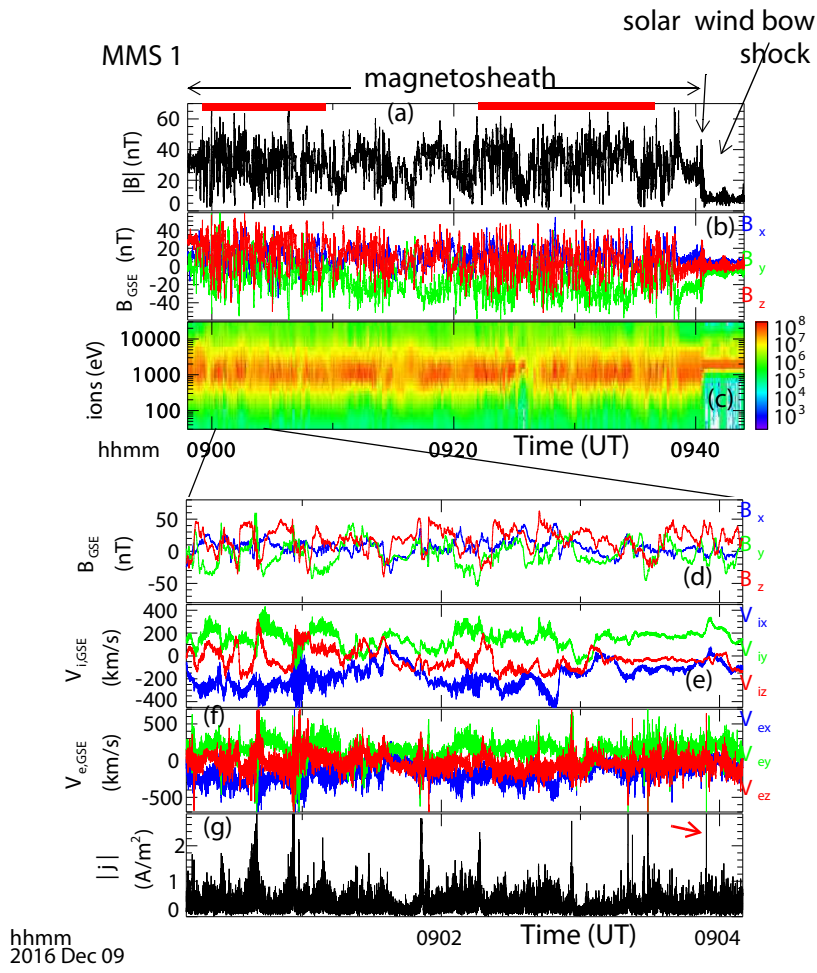


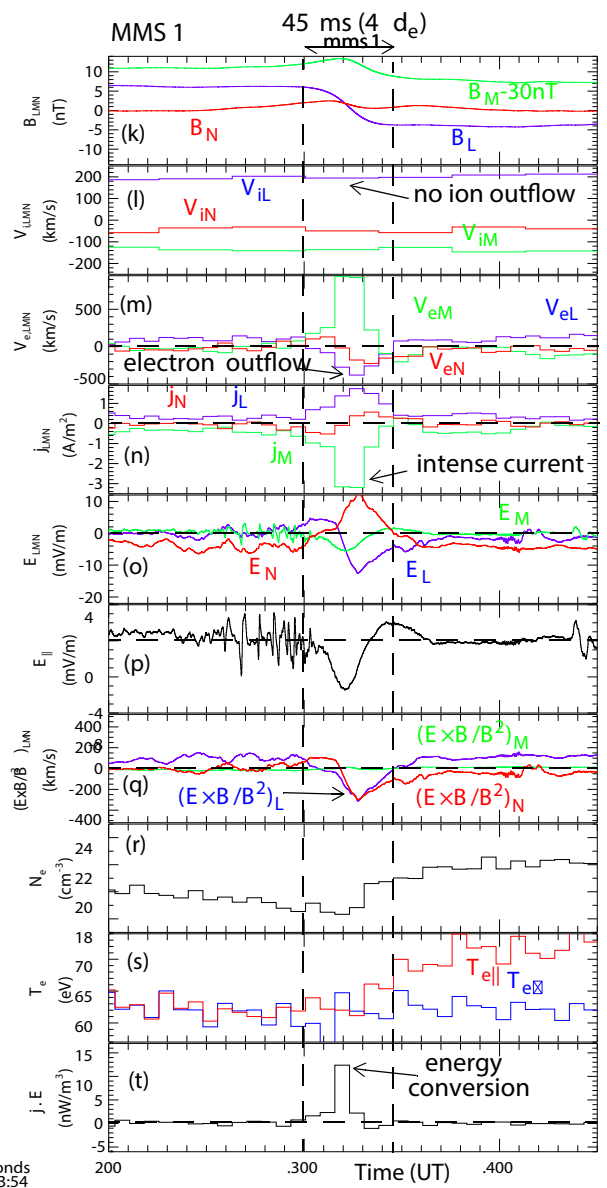
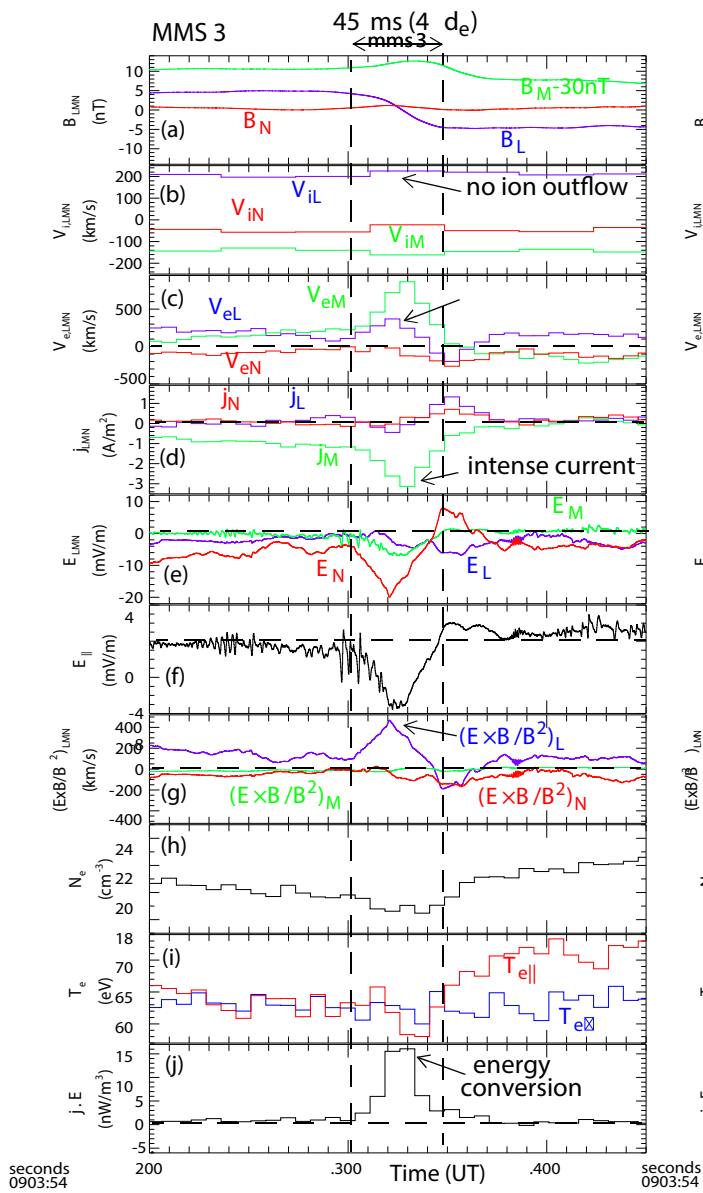
(b) Small-Scale Electron Reconnection

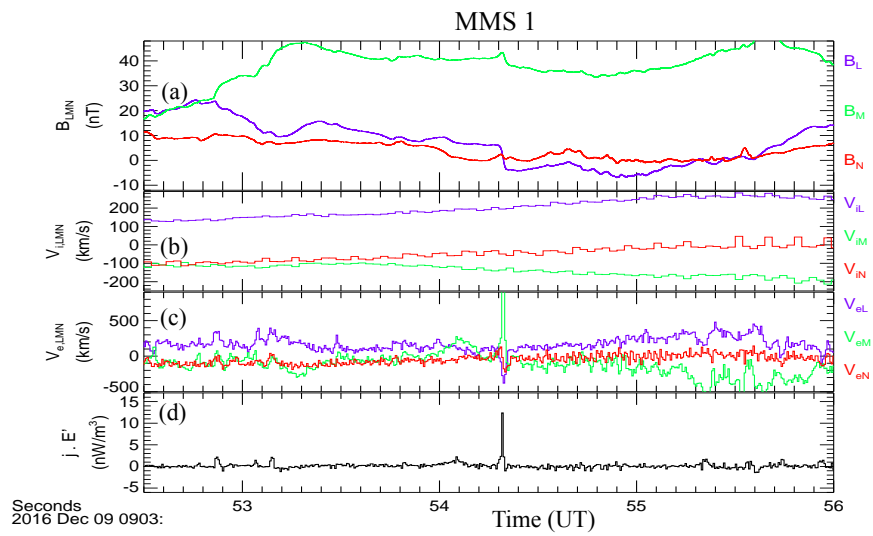


(c)









MMS 1

